

GALAXY DOWNSIZING AND THE REDSHIFT EVOLUTION OF OXYGEN AND NITROGEN ABUNDANCES: ORIGIN OF THE SCATTER IN THE N/H–O/H DIAGRAM

Leonid S. Pilyugin

*Main Astronomical Observatory of National Academy of Sciences of Ukraine, 27
Zabolotnogo str., 03680 Kiev, Ukraine*

pilyugin@mao.kiev.ua

and

Trinh X. Thuan

*Astronomy Department, University of Virginia, P.O. Box 400325, Charlottesville, VA
22904-4325*

txt@virginia.edu

ABSTRACT

The oxygen and nitrogen abundance evolutions with redshift of emission-line galaxies in the Sloan Digital Sky Survey are considered for four intervals of galaxy stellar masses, ranging from $10^{11.3} M_{\odot}$ to $10^{10.2} M_{\odot}$. We have measured their line fluxes and derived the O and N abundances using recent calibrations. The evolution of O and N abundances with redshift clearly shows the galaxy downsizing effect, where enrichment (and hence star formation) ceases in high-mass galaxies at earlier times and shifts to lower-mass galaxies at later epochs. The origin of the scatter in the N/H – O/H diagram has been examined. The most massive galaxies, where O and N enrichment and star formation has already stopped, occupy a narrow band in the N/H – O/H diagram, defining an upper envelope. The less massive galaxies which are still undergoing star formation at the current epoch are shifted downwards, towards lower N/H values in the N/H – O/H diagram. This downward shift is caused by the time delay between N and O enrichment. This time delay together with the different star formation histories in galaxies is responsible for the large scatter in the N/H – O/H diagram.

Subject headings: galaxies: abundances – galaxies: evolution

1. INTRODUCTION

Oxygen and nitrogen are key elements in the study of the chemical evolution of galaxies. The N/O – O/H (or N/H – O/H) diagram has been considered by many authors (e.g. Edmunds & Pagel 1978; Matteucci & Tosi 1985; Pilyugin 1992, 1993; Henry et al. 2000; Gavilán et al. 2006; Izotov et al. 2006). A prominent feature of this diagram is that, in its high-metallicity part ($12+\log(\text{O}/\text{H}) \gtrsim 8.3$), the N/H abundance ratio shows a large scatter at a fixed value of the O/H abundance ratio (Henry et al. 2000; Pilyugin et al. 2003; López-Sánchez & Esteban 2010). The N/H value for a given O/H contains important information about the heavy element enrichment history of a galaxy, and consequently, about its star formation history. Therefore, an explanation of the origin of the scatter in the N/H – O/H diagram is key to understanding the evolution of galaxies.

Two main explanations are presently considered to account for the scatter in normal spiral galaxies: 1) the time delay between nitrogen and oxygen enrichment; and 2) the local enrichment in nitrogen by Wolf-Rayet (WR) stars. Concerning the first explanation, Edmunds & Pagel (1978) have noted that, due the fact that O and N are produced in stars of different masses, there can be a significant time delay between the release of O, produced in high-mass stars, and that of N, produced in intermediate-mass stars, into the interstellar medium (ISM). The N/O ratio of a galaxy then becomes an indicator of the time that has elapsed since the last episode of star formation. Current stellar evolution models predict that N is mainly manufactured and ejected into the ISM by intermediate-mass stars with masses greater than $3\text{-}4M_{\odot}$ (Renzini & Voli 1981; van den Hoek & Groenewegen 1997; Marigo 2001; Gavilán et al. 2005), although massive stars can contribute, at least at low metallicities (Chiappini et al. 2005). This suggests that the time delay between N and O enrichment in galaxies is 250 – 400 Myr, depending on the adopted stellar mass–lifetime relation (Romano et al. 2005). Properties of the observed N/O – O/H diagram can generally be reproduced by chemical evolution models of galaxies by taking into account a time delay (Matteucci & Tosi 1985; Pilyugin 1992, 1993, 1999; Henry et al. 2000; Contini et al. 2002; Gavilán et al. 2006). The exact value of the time delay is however still a subject of debate (Pilyugin et al. 2003; Richer & McCall 2008; Thuan et al. 2010).

Concerning the second explanation, it is known (López-Sánchez & Esteban 2010, and references therein) that some galaxies with WR features have a high N/O ratio. This suggests that the ejecta of WR stars may locally enrich the ISM in N. Henry et al. (2000) noted that most points in the N/O – O/H diagram cluster at relatively low N/O values. This led them to conclude that the lower envelope is the “equilibrium” unperturbed locus and that the observed scatter is the result of intermittent increases in N, caused by the local contamination by WR stars or luminous blue variables. Izotov et al. (2006) also arrived at

the same conclusion.

Selective heavy element loss through enriched galactic winds may also introduce scatter in the N/O ratios. It is believed, however, that galactic winds play an important role in the chemical evolution of only dwarf galaxies, not of giant spirals (e.g. Pilyugin et al. 2004).

In recent years, the number of good-quality spectra of emission-line galaxies has increased dramatically due to the completion of several large spectral surveys, and in particular of the Sloan Digital Sky Survey (SDSS) (York et al. 2000). This opens the possibility of using the SDSS spectral base to study the evolution of O and N abundances in galaxies in the redshift range $z \lesssim 0.4$ (e.g. Tremonti et al. 2004). In a previous study (Thuan et al. 2010), we have considered the evolution of O and N abundances in galaxies with different stellar masses. We have found clear evidence for galaxy downsizing, where the sites of active star formation and hence of metal enrichment shift from high-mass galaxies at early cosmic times to lower-mass systems at later epochs (Cowie et al. 1996). All enrichment ceases in the most massive galaxies at late cosmic times. This downsizing effect provides a remarkable opportunity for clarifying the origin of the scatter in the N/H – O/H diagram. Indeed, if the scatter is caused by a time delay between O and N enrichment in galaxies, then it should be minimized for the most massive galaxies where enrichment has stopped. On the other hand, one should expect that the N/H ratios of the less massive galaxies (those with significant star formation at the current epoch) to be shifted towards lower values relative to the massive galaxies in the N/H – O/H diagram, because there is a time delay between N and O enrichment and N has not yet been released in the ISM.

We examine in this paper whether the time delay is in fact responsible for the large scatter in the N/H – O/H diagram. Our previous study was based on the MPA/JHU catalogs of automatic line flux measurements of the SDSS spectra (see Brinchmann et al. (2004); Tremonti et al. (2004) and other publications of those authors). The accuracy of such automatic line flux measurements seems is not good enough for investigating the origin of scatter in the N/H – O/H diagram. We have thus decided to manually measure the line fluxes of the SDSS spectra. This provides us with more accurate line flux measurements, especially for spectra of objects with the largest redshifts, those with redshifts between 0.3 and 0.4.

2. SAMPLE SELECTION

We first extract from the MPA/JHU catalogs four subsamples of emission-line galaxies, each covering a different interval of galaxy stellar mass, centered respectively on the mass

values $M_S = 10^{11.3}M_\odot$, $10^{11.0}M_\odot$, $10^{10.6}M_\odot$, and $10^{10.2}M_\odot$. To have a reasonable number of galaxies in each subsample and in order for the galaxies to cover the whole redshift range in a roughly uniform fashion, the mass interval dM was chosen to be small and to vary from 0.0015 to 0.10 dex, depending on the redshift and M_S . For each mass interval, we have extracted from the MPA/JHU catalogs emission-line galaxies with automatic measurements of fluxes in the $H\beta$, $H\alpha$, $[\text{O II}]\lambda\lambda 3727, 3729$, $[\text{O III}]\lambda 5007$, $[\text{N II}]\lambda 6584$ emission lines. We impose the additional restrictions that the galaxies have equivalent widths $EW(H\beta) > 10 \text{ \AA}$ (this criterion applies only to galaxies with redshifts < 0.3 , as we did not wish to reduce further the very small number of galaxies with $z > 0.3$), $EW([\text{O II}]\lambda\lambda 3727, 3729) > 3 \text{ \AA}$, $EW([\text{O III}]\lambda 5007) > 3 \text{ \AA}$, and $EW([\text{N II}]\lambda 6584) > 2 \text{ \AA}$. These additional restrictions insure that the chosen galaxies have a reasonably high star formation rate, giving rise to reasonably strong emission lines that can be measured with good accuracy.

Each so chosen spectrum was then examined visually and the noisy spectra were rejected. The line fluxes of the remaining galaxies were then measured with IRAF ¹. The $[\text{O III}]\lambda 5007/H\beta$ vs $[\text{N II}]\lambda 6584/H\alpha$ diagram was then used to reject AGNs (Baldwin et al. 1981), with the dividing line between H II regions ionized by star clusters and AGNs taken from Kauffmann et al. (2003).

The wavelength range of the SDSS spectra is $3800 \text{ \AA} - 9300 \text{ \AA}$, so that for nearby galaxies with redshift $z \lesssim 0.023$, the $[\text{O II}]\lambda 3727 + \lambda 3729$ emission line is out of the observed range. Thus, all galaxies in our total sample have redshifts greater than ~ 0.023 . For distant galaxies with redshift $z \gtrsim 0.33$, the $[\text{S II}]\lambda\lambda 6717, 6731$ emission lines are out of the observed range. The sulfur line intensities are usually used as indicators of the electron density. They serve also to distinguish between hot and warm H II regions, in the framework of the ON calibrations of Pilyugin et al. (2010). Since the sulfur lines are not present, we will assume the electron density to be equal to 100 cm^{-3} and that our sample does not contain hot H II regions (i.e. those with $12 + \log(\text{O}/\text{H}) \lesssim 8.0$). The redshift z and stellar mass M_S of each galaxy were taken from the MPA/JHU catalogs. When the stellar mass of a galaxy with redshift $z > 0.3$ is not available in the MPA/JHU catalogs, we estimated it from its absolute

¹IRAF is distributed by National Optical Astronomical Observatories, which are operated by the Association of Universities for Research in Astronomy, Inc., under cooperative agreement with the National Science Foundation.

magnitude M_z , its colour $m_z - m_r$ and its $H\beta$ equivalent width, using the relation

$$\begin{aligned} \log M_S &= -0.459 M_z - 0.775 (m_z - m_r) + 0.363 + 0.083 \log EW(H\beta) \\ &\textit{for } (m_z - m_r) < -0.3 \end{aligned} \tag{1}$$

$$\begin{aligned} \log M_S &= -0.61 M_z + 0.43 (m_z - m_r) - 2.58 - 0.24 \log EW(H\beta) \\ &\textit{for } (m_z - m_r) > -0.3 \end{aligned}$$

where the galaxy stellar mass M_S is in units of solar masses. This relation was derived by fitting the data for galaxies in the redshift interval $0.3 < z < 0.4$ with available stellar masses in the MPA/JHU catalogs. We caution that this relation is not a general relation for the determination of galaxy stellar masses. It applies only within the small particular redshift interval defined above. We stress also that the derived masses serve only to select galaxies with various masses to populate our different subsamples and are not used in any calculation.

Our final database consists of 221 spectra of galaxies with $M_S = 10^{11.3} M_\odot$ (with 74 objects with M_S derived from Eq. 1), 259 spectra of galaxies with $M_S = 10^{11.0} M_\odot$ (60 objects with M_S from Eq. 1), 244 spectra of galaxies with $M_S = 10^{10.6} M_\odot$ (32 objects with M_S from Eq. 1), and 152 spectra of galaxies with $M_S = 10^{10.2} M_\odot$ (7 objects with M_S from Eq. 1). The measured emission-line fluxes are then corrected for interstellar reddening using the theoretical $H\alpha$ to $H\beta$ ratio, in the same way as in Thuan et al. (2010). O and N abundances are then estimated for each galaxy, using the recent ON calibrations of Pilyugin et al. (2010). These calibrations give both O and N abundances over the whole metallicity range with a satisfactory precision. Pilyugin et al. (2010) found that the mean differences between O abundances determined from these calibrations and from the direct T_e method based on the $[O\text{ III}]\lambda 4363$ line is only ~ 0.075 dex for O abundances, and only ~ 0.05 dex for N abundances.

3. GALAXY DOWNSIZING AND THE ORIGIN OF THE SCATTER IN THE N/H – O/H DIAGRAM

We first check the accuracy of our abundance determinations. Fig.1 shows the N/H – O/H diagram. The gray points represent galaxies in our four SDSS subsamples with O and N abundances derived from the ON calibrations. The dark triangles show H II regions in nearby galaxies (Pilyugin et al. 2010), with O and N abundances derived with the T_e method, commonly thought to be the most accurate one. It is seen that the galaxies in our SDSS subsamples occupy the same region in the N/H – O/H diagram as the H II regions in nearby galaxies with O and N abundances derived through the T_e method. This confirms that our

ON-calibration-based O and N abundances are quite reliable. The remarkable feature to note in the N/H – O/H diagram is the large scatter in N/H values at a given O/H value. This holds as much for SDSS objects as for H II regions in nearby galaxies.

We next investigate the redshift evolution of O abundances in each of the four galaxy mass ranges (Fig.2). In each panel labeled by the galaxies’ masses, the filled gray circles show individual galaxies. The solid line is the best least-squares fit to those data. Inspection of the upper panel shows that there is no systematic variation with redshift of the O abundance in galaxies with masses $\sim 10^{11.3}M_{\odot}$ up to $z = 0.4$. This implies that these galaxies have reached a high astration level some 4 Gyr ago, and have been somewhat ”lazy” in their evolution afterwards. The average value of the O abundances for galaxies with stellar mass $M_S = 10^{11.3}M_{\odot}$ is remarkably close to the O abundance in the Orion nebula ($12+\log(O/H) = 8.51$) obtained by Esteban et al. (2004). It is also in good agreement with the O abundances in nearby luminous galaxies obtained by Moustakas et al. (2010), using the calibration of Pilyugin & Thuan (2005).

Comparison between the different panels of Fig.2 shows clearly the effect of galaxy downsizing. Massive galaxies do not show O enrichment: they already reach a relatively high O abundance at $z = 0.4$, and that abundance remains nearly constant until $z = 0$. The less massive galaxies do show O enrichment: they have lower O abundances at $z = 0.4$, but these increase from $z = 0.4$ to $z = 0$, and at the present epoch, they are nearly the same as in massive galaxies.

We next investigate the origin of the scatter in the N/H – O/H diagram. The upper left panel of Fig.3 shows that diagram for the subsample that contains our most massive galaxies, those with masses $\sim 10^{11.3}M_{\odot}$. It is seen that the scatter in the N/H – O/H diagram for this subsample of galaxies is small, especially for galaxies with $z \lesssim 0.3$ (see Fig. 4, to be discussed later). Using this subsample, we have derived the following relation between N/H and O/H abundances

$$\log(N/H) = 2.596 (\pm 0.118) \log(O/H) - 14.359 (\pm 1.001). \quad (2)$$

This relation has been derived in an iterative manner. First, a least-squares fit was obtained for all data points with $z < 0.3$. Then, objects with deviations larger than 2σ were rejected and a new least-squares fit derived. The final fit is obtained when, after several iterations, the fits for two consecutive ones coincide. The scatter in the N/H values relative to the final fit is $\sigma = 0.037$ dex. The derived N/H – O/H relation is shown in the upper left panel of Fig.3 by a solid line, while the dashed lines show $\pm 2\sigma$ shifts from that relation. It should be noted that this N/H – O/H relation is derived for a relatively small range of O/H and, consequently, its slope cannot be determined with a high precision. Therefore, it should not

be used for O/H values beyond the above specified range. To establish a more general N/H – O/H relation, a sample of objects covering a more extended range in O/H would be needed.

The above relation links N/H and O/H in galaxies where O and N enrichment has already ceased. One would expect that galaxies with significant star formation in the near past would be displaced towards lower N/H values in the N/H – O/H diagram relative to this relation, because of the time delay between N and O enrichment. Comparison between the four panels of Fig.3 clearly shows this effect. The most massive galaxies define an upper envelope in the N/H – O/H diagram and they do not show significant star formation in the last 4 Gyr (Fig.2). The lower-mass galaxies are shifted towards lower N/H values and they show significant star formation during the same period (Fig.2). This is solid evidence that the differences in N/H for galaxies with a given O/H are caused by the time delay between N and O enrichment.

Fig.4 shows how the deviations of the N abundance from the N/H – O/H relation (Equation 2) vary with mass and redshift. The gray points represent individual galaxies. The dashed lines show $\pm 2\sigma$ deviations from that relation. The N evolution with redshift in galaxies of different masses is clearly due to a galaxy downsizing effect. As the universe ages, the sites of star formation shift from high-mass galaxies ($\log M = 11.3$), where star formation and O and N enrichment have ceased more than 4 Gyr ago, to lower-mass galaxies ($\log M < 11.3$) where active star formation and O and N enrichment are still ongoing. Comparison of Figs.4 and 2 shows that the downsizing effect is more prominent for N than for O. This is because N is a secondary element while O is a primary one.

To have comparable numbers of galaxies with low redshifts ($0.02 < z < 0.15$) in the highest-mass subsample of galaxies ($M_S = 10^{11.3} M_\odot$) and in the lowest-mass subsample ($M_S = 10^{10.2} M_\odot$), we had to use a mass interval $dM = 0.10$ in the first case, and a value about 66 times lower, $dM = 0.0015$, in the second case. This implies that, at the current epoch, star formation events occur nearly two orders of magnitude more often in low-mass galaxies than in high-mass ones. Because of the time delay between O and N enrichment, there is a downward shift towards lower N/H values for low-mass galaxies in the N/H – O/H diagram (Fig.4). This naturally explains the finding of Henry et al. (2000) that most of the local dwarf star-forming galaxies cluster at relatively low N/O values in the N/O – O/H diagram.

4. CONCLUSIONS

The O and N abundance evolutions with redshift in emission-line galaxies from the Sloan Digital Sky Survey (SDSS) are investigated. To investigate the galaxy downsizing

effect, we have measured line fluxes of selected galaxies in four intervals of galaxy stellar masses, ranging from $10^{11.3} M_{\odot}$ to $10^{10.2} M_{\odot}$. The O and N abundances have been derived using the recent accurate calibrations of Pilyugin et al. (2010).

We have found that the O and N abundance evolutions with redshift of the galaxies in our sample clearly show the galaxy downsizing effect (Cowie et al. 1996), where enrichment (and hence star formation) is shifted from high-mass galaxies at earlier cosmic times to lower-mass galaxies at later epochs.

We have examined the origin of the scatter in the N/H – O/H diagram. We have found that the most massive galaxies where O and N enrichment and star formation has already stopped, occupy a narrow band in the N/H – O/H diagram, defining an upper envelope. On the other hand, the less massive galaxies with significant star formation at the current epoch are shifted downwards, towards lower N/H values. The scatter of N/H for a given O/H is caused by the time delay between N and O enrichment and the different star formation histories in different galaxies.

Acknowledgments

L.S.P. thanks the hospitality of the Astronomy Department of the University of Virginia. He acknowledges the support of the Cosmomicrophysics project of the National Academy of Sciences of Ukraine. T.X.T. thanks the support of NASA.

REFERENCES

- Baldwin, J.A., Phillips, M.M., & Terlevich, R. 1981, *PASP*, 93, 5
- Brinchmann, J., Charlot, S., White, S.D.M., Tremonti, C., Kauffmann, G., Heckman, T., & Brinkmann, J. 2004, *MNRAS*, 351, 1151
- Chiappini, C., Matteucci, F., & Ballero, S.K. 2005, *A&A*, 437, 429
- Contini, T., Treyer, M.A., Sullivan, M., & Ellis, R.S. 2002, *MNRAS*, 330, 75
- Cowie, L.L., Songaila, A., Hu, E.M., & Cohen, J.G. 1996, *AJ*, 112, 839
- Edmunds, M.G., & Pagel, B.E.J. 1978, *MNRAS*, 185, 77P
- Esteban, C., Peimbert, M., Carcía-Rojas, J., Ruiz M.T., Peimbert, A., & Rodríguez M. 2004, *MNRAS*, 355, 229

- Izotov, Y.I., Stasińska, G., Meynet, G., Guseva, N.G., & Thuan, T.X.. 2006, *A&A*, 448, 955
- Gavilán, M., Buell, F., & Mollá, M. 2005, *A&A*, 432, 861
- Gavilán, M., Mollá, M., & Buell, F. 2006, *A&A*, 450, 509
- Henry, R.B.C., Edmunds, M.G., & Kóppen, J. 2000, *ApJ*, 541, 660
- Kauffmann, G., Heckman, T.M., Tremonti, C., & et al. 2003, *MNRAS*, 346, 1055
- López-Sánchez, Á.R., & Esteban, C. 2010, *A&A*, 517, A85
- Marigo P. 2001, *A&A*, 370, 194
- Matteucci, F., & Tosi, M. 1985, *MNRAS*, 217, 391
- Moustakas, J., Kennicutt, R.C., Tremonti, C.A., Dale, D.A., Smith, J.-D.T., & Calzetti, D. 2010, *ApJS*, 190, 233
- Pilyugin, L.S. 1992, *A&A*, 260, 58
- Pilyugin, L.S. 1993, *A&A*, 277, 42
- Pilyugin, L.S. 1999, *A&A*, 346, 428
- Pilyugin, L.S., & Thuan, T.X. 2005, *ApJ*, 631, 231
- Pilyugin, L.S., Thuan, T.X., & Vílchez, J.M. 2003, *A&A*, 397, 487
- Pilyugin, L.S., Vílchez, J.M., & Contini, T. 2004, *A&A*, 425, 849
- Pilyugin, L.S., Vílchez, J.M., & Thuan, T.X. 2010, *ApJ*, 720, 1738
- Renzini, A., & Voli, M. 1981, *A&A*, 94, 175
- Richer, M.G., & McCall, M.L. 2008, *ApJ*, 684, 1190
- Romano, D., Chiappini C., Matteucci, F. & Tosi, M. 2005, *A&A*, 430, 491
- Thuan, T.X., Pilyugin, L.S., & Zinchenko, I.A. 2010, *ApJ*, 712, 1029
- Tremonti, C.A., Heckman, T.M., Kauffmann, G., & et al. 2004, *ApJ*, 613, 898
- van den Hoek, L.B., & Groenewegen, M.A.T. 1997, *A&AS*, 123, 305
- York, D.G., et al. 2000, *AJ*, 120, 1579

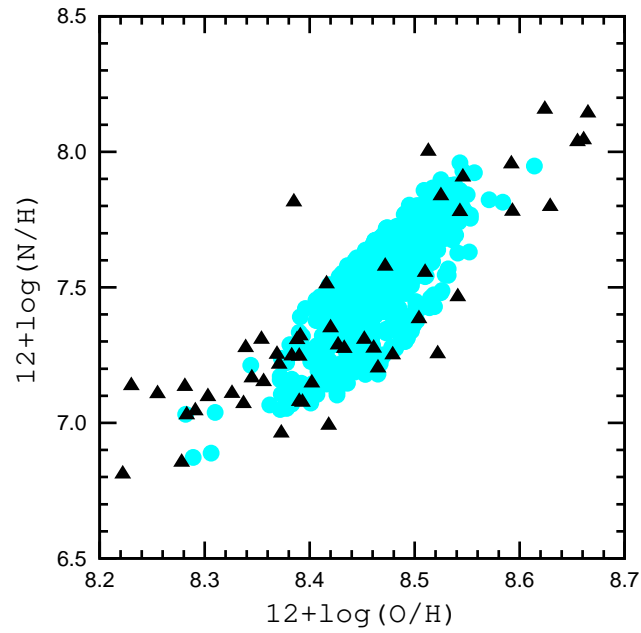


Fig. 1.— The N/H – O/H diagram. The gray (light-blue in the electronic version) points represent individual galaxies from our four SDSS subsamples with oxygen and nitrogen abundances derived from the ON calibrations of Pilyugin et al. (2010). The dark (black in the electronic version) triangles show H II regions in nearby galaxies (from a compilation of Pilyugin et al. (2010) with oxygen and nitrogen abundances derived with the T_e method. (A color version of this figure is available in the online journal)

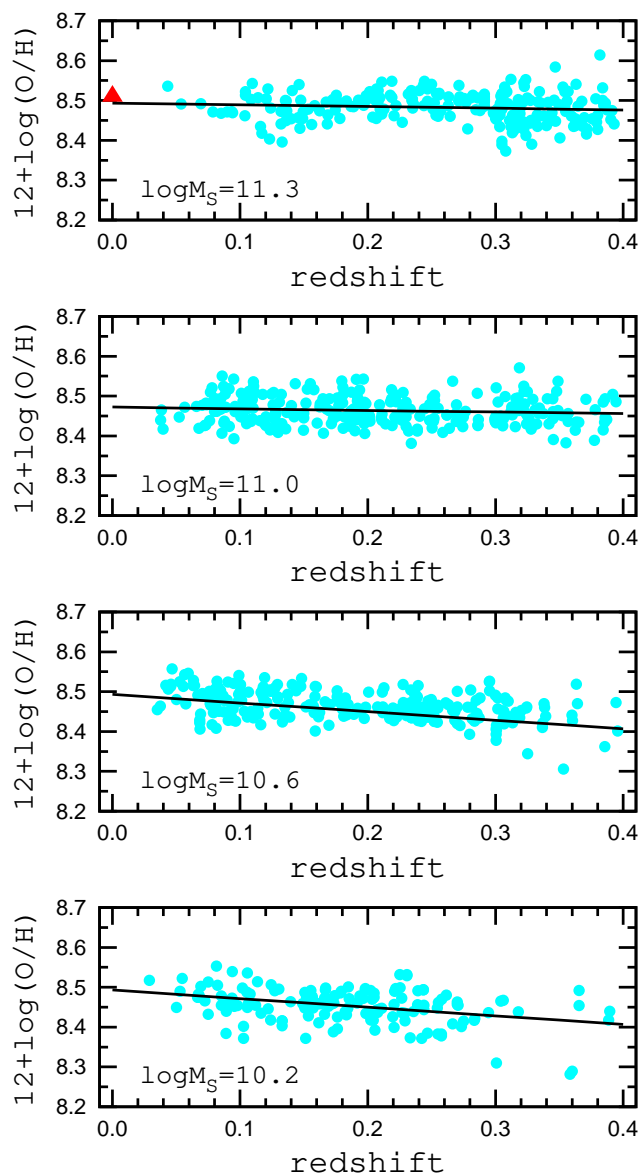


Fig. 2.— Oxygen abundances as a function of redshift for the four subsamples of galaxies with different stellar masses. In each panel, labeled by the galaxy stellar mass, the gray (light-blue in the electronic version) points represent individual galaxies. The solid (black in the electronic version) line is the least-squares best fit to those data. The dark (red in the electronic version) filled triangle in the top panel shows the Orion Nebula. (A color version of this figure is available in the online journal)

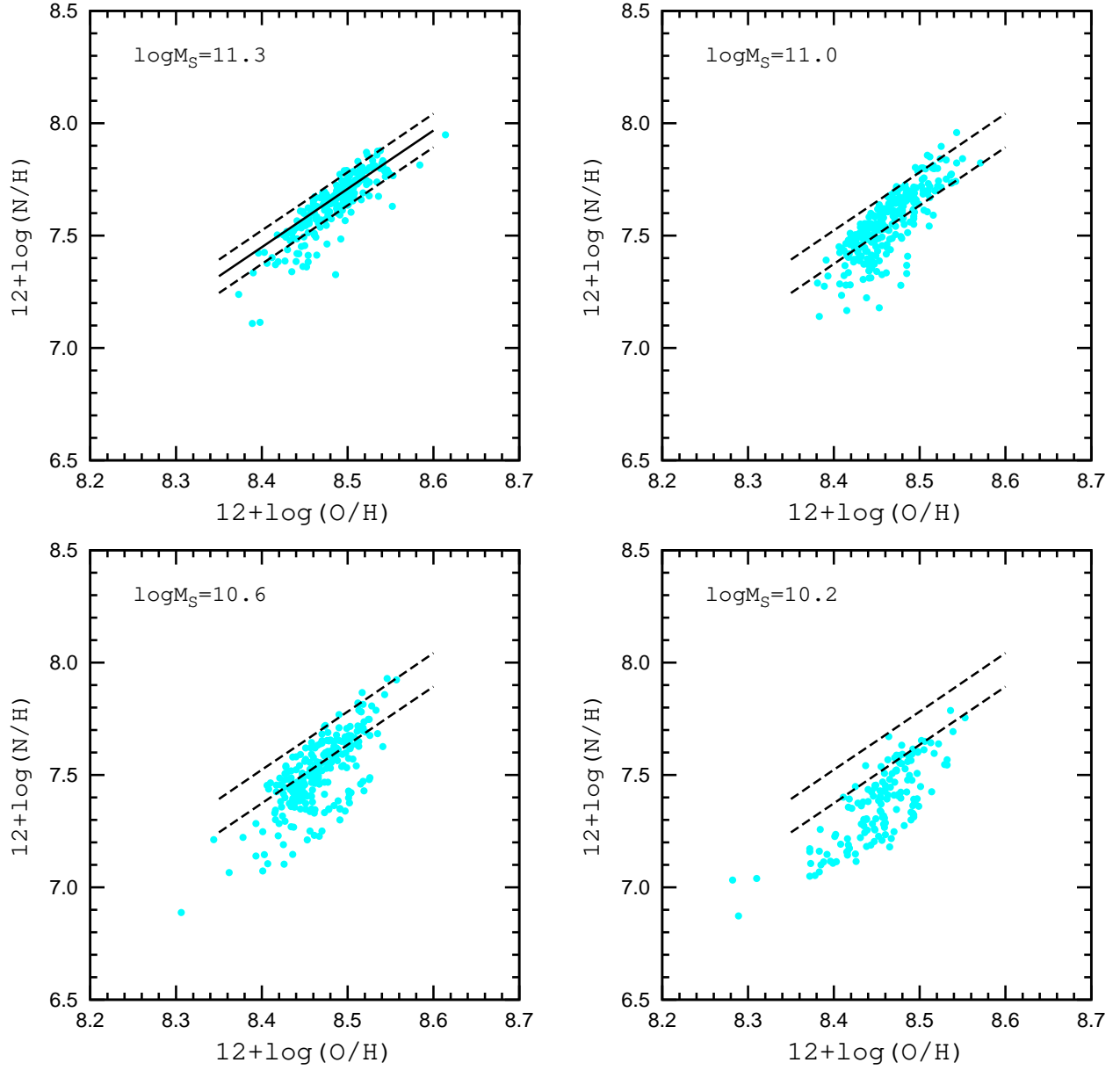


Fig. 3.— N/H – O/H diagrams for the four subsamples of galaxies with different stellar masses. In each panel, labeled by the galaxy stellar mass, the gray (light-blue in the electronic version) points represent individual galaxies. The solid (black in the electronic version) line in the left upper panel is the derived N/H – O/H relation (equation 2) for the most massive galaxy subsample, with masses $\sim 10^{11.3}M_{\odot}$. The dashed (black in the electronic version) lines show the $\pm 2\sigma$ shifts from this relation. These dashed lines are reproduced in all other panels. (A color version of this figure is available in the online journal)

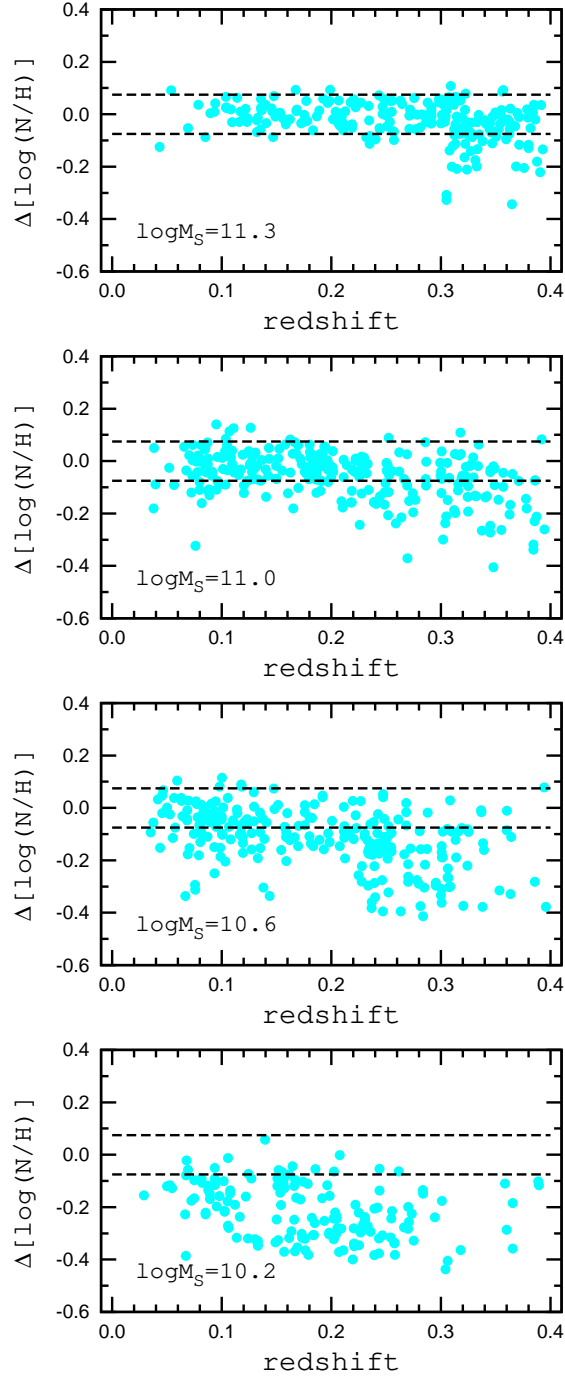


Fig. 4.— Deviations of the nitrogen abundance from the N/H–O/H relation, derived for the most massive galaxy subsample (equation 2), as a function of redshift for all four subsamples of galaxies with different stellar masses. In each panel, labeled by the galaxy stellar mass, the gray (light-blue in the electronic version) points represent individual galaxies. The dashed (black in the electronic version) lines show the $\pm 2\sigma$ deviations from the N/H–O/H relation. (A color version of this figure is available in the online journal)